Neurosci Bull October 1, 2011, 27(5): 287–299. http://www.neurosci.cn
DOI: 10.1007/s12264-011-1736-7

·Original Article·

The origin and development of plaques and phosphorylated tau are associated with axonopathy in Alzheimer's disease

Ai-Wu Xiao[1], Jing He[1], Qian Wang[1,2], Yi Luo[1], Yan Sun[1], Yan-Ping Zhou[1], Yang Guan[3], Paul J. Lucassen[2], Jia-Pei Dai[1]

[1]*Wuhan Institute for Neuroscience and Neuroengineering, South-Central University for Nationalities, Wuhan 430074, China*

[2]*Swammerdam Institute for Life Sciences, Center for Neuroscience, University of Amsterdam, Amsterdam 1098XH, the Netherlands*

[3]*Department of Ultrapathology, Tongji Medical College of Huazhong University of Science & Technology, Wuhan 430030, China*

Abstract: Objective The production of neurotoxic β-amyloid and the formation of hyperphosphorylated tau are thought to be critical steps contributing to the neuropathological mechanisms in Alzheimer's disease (AD). However, there remains an argument as to their importance in the onset of AD. Recent studies have shown that axonopathy is considered as an early stage of AD. However, the exact relationship between axonopathy and the origin and development of classic neuropathological changes such as senile plaques (SPs) and neurofibrillary tangles (NFTs) is unclear. The present study aimed to investigate this relationship. **Methods** Postmortem tracing, combined with the immunohistochemical or immunofluorescence staining, was used to detect axonopathy and the formation of SPs and NFTs. **Results** "Axonal leakage"–a novel type of axonopathy, was usually accompanied with the extensive swollen axons and varicosities, and was associated with the origin and development of Aβ plaques and hyperphosphorylated tau in the brains of AD patients. **Conclusion** Axonopathy, particularly axonal leakage, might be a key event in the initiation of the neuropathological processes in AD.

Keywords: Alzheimer's disease; axonopathy; senile plaques; neurofibrillary tangles; postmortem tracing

1 Introduction

Alzheimer's disease (AD) is a debilitating neurodegenerative disease and is the most common form of dementia. The pathological hallmarks of AD are senile plaques (SPs) and neurofibrillary tangles (NFTs), which are potentially linked to alterations of the axonal compartment. SPs are mainly composed of β-amyloid (Aβ) and dystrophic neuritis. Some dystrophic neuritis correspond to axonal swellings, which often contain abnormal accumulations of axonal cargos and phosphorylated tau[1]. NFTs are related to the abnormal phosphorylation of the microtubule-associated protein tau and its subsequent dislocation from axons to the presynaptic terminals and somatodendritic compartments[2]. Although neurotoxic Aβ deposition and the formation of hyperphosphorylated tau are thought to be critical steps involved in the neuropathological mechanisms of AD, a debate still exists over whether SPs or NFTs play a key and causal role in the neuropathological mechanisms of AD. Much effort has been made to

Corresponding author: Jia-Pei Dai
Tel: +86-27-67841165; Fax: +86-27-67840917
E-mail: jdai@mail.scuec.edu.cn
Article ID:1673-7067(2011)05-0287-13
Received date: 2011-07-17; Accepted date: 2011-08-20

find a direct neuropathological relationship between SPs and NFTs or to look for additional evidence supporting an alternative proposal that both SPs and NFTs may be the results of neuropathological changes, not the causes of AD. However, there is currently no consensus on this issue[3-14].

The biological function of a neuron is highly dependent on an intact axon through which axonal transport and neural signals are supported[15,16]. In AD, obvious axonopathy mainly manifests as impairment of axonal transport and swelling of the axon and varicosity[17-21]. Such axon defects have been shown to precede known disease-related pathology in mouse models of AD, and are considered as early stages of AD[19]. A previous study has found that the decrease in axonal transport in the cortical neurons in AD is related to the degree of the classic neuropathological changes, SPs and NFTs[17]. Axonal transport impairment and the swelling of axons and varicosities have also been observed both in living AD patients and in animal models[21-27].

Although these studies imply that axonopathy plays an important and early role in the neuropathological mechanisms of AD, it remains still unclear whether axonopathy is an independent neuropathological change parallel to the formation of SPs and NFTs, or whether it plays an additional role in AD. In a preliminary study[28], we identified a new type of axonopathy named "axonal leakage" in AD. The present study aimed to investigate its relationship with the origin and formation of SPs and NFTs in AD.

2 Materials and methods

2.1 Human brain materials Human brain tissues were obtained from the Netherlands Brain Bank (NBB). According to the protocol of the NBB, specific permission for brain autopsy and use of the brain tissue and the medical records for research purpose was given by the patients or their partners/relatives. AD was clinically diagnosed based on the criteria of the National Institute of Neurological and Communication Disorders and the Stroke-Alzheimer's disease and Related Disorders Association[29]. The diagnosis of "probable AD" was established by excluding other causes of dementia. Brains from AD patients and controls were systematically neuropathologically investigated. Neuropathological changes in AD were scored using the staging system of Braak[30]. The clinical diagnosis of "probable AD" was confirmed by a Braak score of IV or more, while non-demented aged and other subjects were at Braak stages 0–II.

A total of 39 postmortem human brains were collected for the present study, 26 of which were from people with AD. The clinical and neuropathological data of the subjects were listed in Table 1. The average age and postmortem delay were 83.7 years and 4:09 (hours:minutes) for AD, and 67.8 years and 9:03 for no-demented subjects, respectively. Following removal of the brain, standardized samples of gyrus from the anterior part of the medial frontal cortex (FC, equivalent to Broca's area 9), medial temporal cortex (TC, equivalent to Broca's area 21), occipital cortex (OC, equivalent to Broca's area 7) and hippocampus were dissected. The cortex samples were trimmed into slices (0.4–0.6 cm thick) containing the cortical layers and 1.5–2.0 cm white matter. The hippocampus was cut into coronal slices (0.4–0.6 cm thick) containing dentate gyrus, C1–C4 regions and part of the entorhinal cortex.

2.2 Postmortem tracing in human brain slices Postmortem tracing for human brain tissue has been described in a previous study[31]. Briefly, the prepared brain slice was immediately incubated in modified artificial cerebrospinal fluid (M-ACSF) containing (in mmol/L): sucrose 252, KCl 3, $NaHCO_3$ 26, NaH_2PO_4 1.4, and *D*-glucose 10 (pH 7.4) at 0–4 ºC for 1.5–2.0 h. Then the tissue was put onto a small plate, which was placed on a large plate with ice. The injection areas were viewed under an operating microscope. A glass micropipette (tip diameter, 40 μm) with 5% biotinylated dextran amine (BDA, molecular weight 10 000; Molecular Probes, Leiden, The Netherlands) in Tris-buffered saline (TBS, containing 0.05 mol/L Tris and 0.9% NaCl, pH 7.6) was mounted on a micromanipulator and inserted into the slice to a depth of 2 mm (cortical layers III–V). Iontophoretic injection of the tracer was made with

Table 1. Clinical and neuropathological data of AD and non-demented (NS) subjects, and the intensity of SPs and NFTs in the frontal and temporal cortex, and hippocampus

NBBn	Age (y)	Sex	Bw (g)	Pmd (h:m)	CSF (pH)	ApoE	Braak	FC		TC		Hi		DNC
								SPs	NFTs	SPs	NFTs	SPs	NFTs	
95-015	78	F	1005	5:15	6.75	43	6	3	3	3	3	3	3	AD, Aspiration
95-023	66	F	1134	6:53	6.53	44	6	2	3	3	3	3	3	AD, Pneumonia
95-024	88	F	1144	6:55	6.55	43	6	2	1	3	3	3	3	AD, Cardiac decompensation
95-053	79	F	1201	4:10	6.13	43	6	1	1	3	3	3	3	AD, Cachexia and dehydration
95-082	94	F	1295	5:50	6.70	43	4	1	1	2	2	3	3	AD, Cachexia and dehydration
95-087	69	F	1150	4:00	7.28	33	6	3	1	3	3	3	3	AD, Pneumonia
95-103	69	M	1362	2:55	7.20	44	5	3	3	3	3	3	3	AD, Bronchopneumonia
95-114	79	F	799	4:25	6.74	44	6	3	3	3	3	3	3	AD, Cachexia and dehydration
96-006	90	F	1154	3:10	6.69	43	5	2	3	3	3	3	3	AD, Cachexia and dehydration
96-053	91	M	1158	4:15	6.75	33	4	1	1	2	2	2	3	AD, Pneumonia
96-054	87	F	1010	6:55	6.96	43	5	1	1	2	2	3	3	AD, Heart failure
96-061	84	F	1196	3:55	6.64	33	4	2	2	3	3	3	3	AD, Heart failure
96-063	82	F	1385	3:50	7.45	43	5	2	2	3	3	3	3	AD, Pulmonary embolism
96-066	91	F	949	4:35	6.55	43	6	1	3	3	3	3	3	AD, Pneumonia and cachexia
96-070	83	F	1007	4:00	6.73	43	5	1	1	2	2	3	3	AD, Dehydration
96-072	84	F	1021	3:20	6.68	33	5	1	1	2	3	3	3	AD, Cachexia and dehydration
96-110	80	F	1195	5:45	6.51	43	6	1	2	3	3	3	3	AD, Pneumonia
96-115	92	F	964	2:50	6.64	33	5	2	2	3	3	3	3	AD, Cachexia and dehydration
96-123	88	F	1004	3:20	6.52	ND	4	1	1	2	3	3	3	AD, Cachexia
96-130	87	F	955	4:00	6.91	43	4	1	1	3	3	3	3	AD, Dehydration
96-131	87	F	1368	4:05	6.71	33	3	2	0	3	1	3	3	AD, Pneumonia and cachexia
97-012	84	F	1218	3:40	6.43	33	5	2	1	3	3	3	3	AD, Urinary tract infection, marasmus
97-020	87	F	1092	2:55	6.85	43	5	2	2	3	3	3	3	AD, Dehydration
97-056	71	F	1024	3:30	7.10	43	5	3	3	3	3	3	3	AD, Dehydration
97-086	101	F	1016	4:25	6.93	33	4	1	1	1	3	3	3	AD, Cachexia and dehydration
97-091	85	F	1100	2:00	7.25	43	5	1	2	1	3	3	3	AD, Cachexia and dehydration
95-007	54	M	1335	9:10	6.89	32	0	0	0	0	0	0	0	NS, Carotid artery bleeding
95-020	51	F	1348	4:20	6.94	ND	0	0	0	0	0	0	0	MD, Euthanasia
95-084	72	M	1370	7:20	6.61	33	0	2	0	0	0	0	0	NS, Lung emphysema, bronchochitis
95-093	78	M	1440	7:00	6.96	33	1	1	0	2	2	0	1	NS, Decompensation cordis
95-102	53	M	1383	10:00	7.21	43	0	0	0	0	0	0	0	NS, Dissection of the ascending aorta
96-014	54	F	1257	8:00	6.45	33	0	0	0	0	0	0	0	NS, Acute renal failure
96-051	71	F	1256	4:50	6.65	43	2	3	0	3	2	3	3	NS, Cardiac arrest during operation
96-067	70	F	1157	10:30	ND	33	1	0	0	0	0	1	0	NS, Metastasized mamma carcinoma
96-078	87	F	1315	8:00	6.91	33	2	1	0	1	0	1	1	NS, Heart failure
96-081	61	F	1311	5:15	ND	32	0	0	0	0	0	0	0	NS, Glioblastoma multiform, coma
96-084	78	F	1330	7:30	6.60	43	2	0	0	0	1	0	1	NS, Pulmonary emphysema
96-085	84	M	1367	9:00	6.20	33	1	0	1	0	0	0	3	NS, Heart failure, uraemia
97-005	69	F	1276	7:10	6.80	43	2	3	0	3	1	3	1	NS, Chronic myeloid leukaemia

The average age and postmortem delay were 83.7 years and 4:09 (hours:minutes) for AD, and 67.8 years and 9:03 for no-demented subjects, respectively. SPs: senile plaques; NFTs: neurofibrillary tangles; NBBn: Netherlands Brain Bank number; M: male; F: female; Bw: brain weight; Pmd: postmortem delay; h:m: hours: minutes; ApoE: apolipoprotein gene type; Braak: Braak stage; FC: prefrontal cortex; TC: temporal cortex; Hi: hippocampus; AD: Alzheimer's disease; MD: motor neuron disease; NS: non-demented subjects; DNC: diagnosis, neuropathology and cause of death; ND: not detected.

a constant current voltage device using a 7 μA positive current at 50 mV with 7 s on/7 s off duty cycles over 1.5 min. M-ACSF was used in the small plate during tracer injection to keep the tissue moist. After injection, the tissue was put back in M-ACSF and maintained for about 20 min. After that, the tissue was incubated in a beaker containing 300 mL ACSF (in mmol/L: NaCl 120, KCl 3, $CaCl_2$ 1.0, $MgSO_4$ 1.0, $NaHCO_3$ 26, NaH_2PO_4 1.4, *D*-glucose 10, pH 7.3) at room temperature (22 ºC) for 12 h, with a constant supply of 95% O_2 + 5% CO_2 by a membrane oxygenator placed in the ACSF. After incubation, the tissue was fixed in 4% paraformaldehyde in 0.1 mol/L phosphate buffer (pH 7.4) for 3 d. After fixation, the tissue was placed in 20% sucrose in the same buffer for 1 d for cryoprotection, followed by being sectioned, frozen and serially cut on a cryostat (35 μm in thickness). Sections were collected in 0.05 mol/L TBS in sequential order in 2 vials for each brain slice. Sections were treated with 100% methanol followed by 3% H_2O_2, each for 10 min, to reduce endogenous peroxidase activity. For long-term preservation, sections can be stored at 0–4 ºC in 50% glycerol diluted with 0.05 mol/L TBS. For tracer detection**,** the sections were incubated with the avidin-biotin complex (1:800; Vector Laboratories, Inc.; Burlingame, CA, USA) in a mixture of 0.05 mol/L Tris, 0.9% NaCl, 0.25% gelatin, and 0.5% Triton-X 100 (pH 7.4) for 2 h at room temperature. After several rinses with TBS, the sections were incubated with 0.05% 3,3'-diaminobenzidine tetrahydrochloride (DAB), 0.2% nickel-ammonium sulphate, and 0.003% H_2O_2 in 0.05 mol/L TBS (pH 7.4), mounted on gelatin-coated slides, and then dehydrated, cleared, and coverslipped.

2.3 Double immunohistochemical and immunofluorescence staining The double staining combining tracer detection with immunocytochemistry was performed according to the procedures described previously[31]. After visualization of the tracer with DAB + nickel-ammonium sulphate, some cortical sections were processed for immunocytochemical detection of Aβ42 or tau with the ABC Elite detection method (Vector; Burlingame, CA, USA). The primary antibodies used included rabbit polyclonal antibody against Aβ42 (1:500; Bioss; Beijing, China), the specificity and sensitivity of which to identify Aβ deposits and plaques were tested in the brain sections from AD brains and an APP/PS1 transgenic mouse model, rabbit polyclonal phosphospecific antibody (P-tau) recognizing tau when Ser199 and Ser202 are phosphorylated (1:5 000; Biosource; Carlsbad, CA, USA), tau-5 monoclonal antibody reacting with nonphosphorylated tau and the phosphorylated form of tau (1:5 000; Biosource), and anti-human PHF-tau monoclonal antibody (AT8) reacting with an epitope including phosphorylated Ser202 and Thr205 residues (1:10 000; Pierce; Appleton, WI, USA).

The double immunocytochemical staining for Aβ42 and tau in human brain sections was performed in a similar fashion to that described above. After finishing the immunocytochemical staining for P-tau, tau-5 or AT8 with DAB + nickel-ammonium sulphate, immunocytochemical staining for Aβ42 was conducted and the end products were visualized with DAB.

Sections were processed for double immunofluorescence staining of tracer and Aβ42 or tau. Briefly, the sections were first incubated with antibodies anti-Aβ42, P-tau, tau5 or AT8 (dilutions as above) overnight at 4 ºC. Sections were rinsed in PBS for 30 min and incubated in a mixture of FITC-conjugated avidin (1:800; Pierce) and rodamine-conjugated goat anti-rabbit IgG (1:200) (for P-tau and Aβ42) or goat anti-mouse IgG (1:200; Pierce) (for tau-5 and AT8). The sections were washed and mounted on slides with immunofluorescence mounting medium. The staining was examined on a laser scanning confocal microscope (Nikon, Japan) or a fluorescence microscope (Nikon, 90i, Japan). Cross-reactivity was tested by omitting the secondary antibodies for immunostaining, and no staining was detected.

2.4 Electron microscopy A pre-embedding tracer detection technique was used to demonstrate the subcellular distribution of tracer as described before[32]. After tracer staining was finished, the sections displaying satisfactory staining were post-fixed in 1.5% osmium tetroxide/1% ferricyanide in 0.1 mol/L sodium cacodylate buffer for 30 min, dehydrated in a series of graded ethanols, and flat-embedded in epoxy resin. Ultrathin sections (90–160 nm)

were cut and photographed using a Philips 201 electron microscope (Philips Industries, Eindhoven, The Netherlands) at 60 kV. Counterstaining was omitted in order to visualize deposited DAB granules (a dot-like configuration).

2.5 Semi-quantitative analysis of neuropathological changes in AD brains and controls A semi-quantitative score of the numbers of SPs and NFTs was performed in FC and TC with Bodian staining in 6-μm paraffin sections according to the standard protocol of the NBB. Changes were scored separately in each brain area in the following way: 0: absent; 1: sparse/slight but less than moderate; 2: moderate, 2–3 NFTs or SPs per 0.4 mm^2; 3: frequent/severe, more than moderate[17].

2.6 Quantitative analysis of axonal leakage in frontal and temporal cortex in AD brains and controls All sections from a single human brain slice in each case were collected in sequential order in 2 vials and one vial was used to perform tracer staining. Therefore, all sections containing a tracer-labeled injection spot (about 30 sections in each slice) were processed to measure the number of instances of axonal leakage in the tracer-labeled fibers projecting to white matter using a motorized microscope (ECLIPSE 90i, Nikon, Japan) equipped with a Nikon cooled color CCD camera (DS-5MC-U2) and controlled by Nikon image analysis software (NIS-Elements BR 3.1). The number of instances of axonal leakage was counted in a 200× microscopic visual field in each section. Diffuse tracer staining around axons or varicosities was considered typical of axonal leakage, and each instance was scored. This method of measuring axonal leakage is based on the principles of stereology. The investigator was blind to case type during the quantitative analysis.

2.7 Statistical analysis The measured values from 8 sections containing the largest number of instances of axonal leakage among all measured sections in each human brain slice were used for statistical analysis. Statistical analysis of significant differences in the mean values between FC and TC in AD or non-demented aged group was conducted by the paired *t*-test (two-tailed). $P < 0.05$ was considered statistically significant.

3 Results

3.1 Typical morphological characteristics of axonal leakage at light and electron microscopic levels in the brains of AD patients Using a postmortem tracing technique with BDA as the tracer, the axonal changes in the frontal and the temporal cortices were examined in 39 postmortem human brains, 26 of which were clinically diagnosed as probable AD and confirmed by neuropathological exams (Table 1). As shown in Fig. 1A–C, swollen axons and varicosities were observed in brain areas affected by AD as reported earlier[19]. Unexpectedly, in AD brains, tracer staining was observed around certain areas of swollen axons, or around the edges of swollen varicosities (Fig. 1A–C), while the morphology of the labeled fibers was almost normal in young control brains (Fig. 1D) and in postmortem rat brains[31]. This axonal change was named "axonal leakage", a new type of axonopathy[28]. Fig. 2A and Fig. 2B present the typical instances of swollen axons and varicosities, and axonal leakage at the light microscopic level, respectively. The theoretical explanation of axonal leakage identification using this tracing technique and the use of this terminology is provided in Fig. 3.

Sections displaying axonal leakage were selected by light microscopy and were further examined under the electron microscope. In leaking axons, the staining for tracer (a dot-like configuration) was observed in the intra-axonal and extra-axonal spaces and even in the myelin sheath (Fig. 4A), while in intact axons, the staining was only restricted to the intra-axonal space (Fig. 4B).

3.2 Degrees of axonal leakage in frontal and temporal cortex in AD and control brains Different brain areas in AD and in non-demented aged subjects were examined to determine whether there was any difference in the amount of axonal leakage. The number of instances of axonal leakage (the number of sites with diffuse tracer staining) was quantitatively analyzed by comparing FC with TC in 8 AD (average age, 86.9 years) and 4 non-demented subjects (NS; average age, 79.6 years). This analysis excluded the effects of several factors related to the use of materials

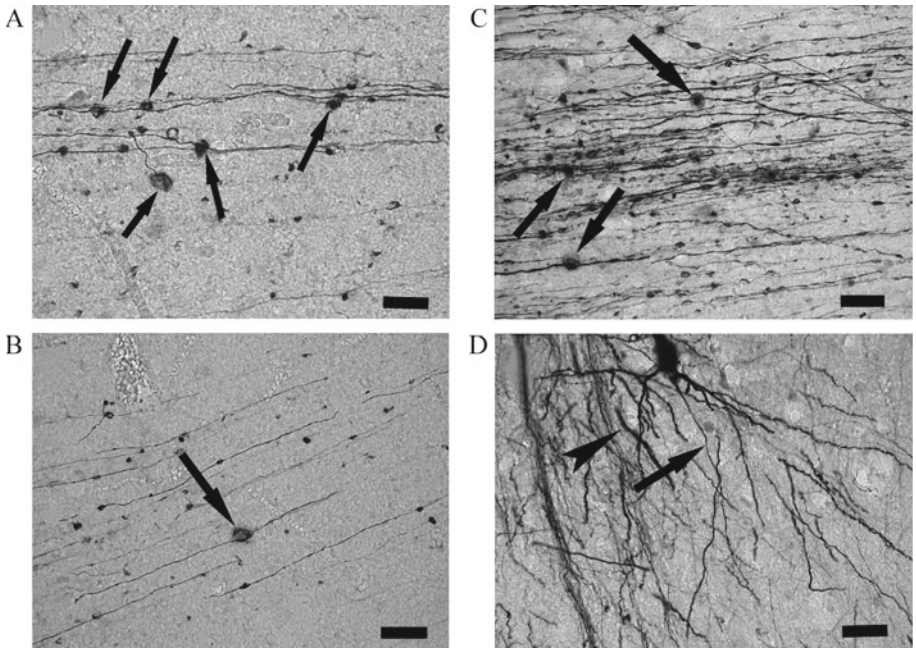

Fig. 1 Postmortem tracing showed swollen axons and varicosities as well as axonal leakage in Alzheimer's disease (AD) brains. A: Labeled fibers in the temporal cortex (TC) of an AD brain showed instances of axonal leakage (diffuse staining, arrows) from slightly swollen fibers. B: A typical example of axonal leakage in TC (arrow). C: Many swollen fibers and different sizes of leaking varicosities in TC of an AD brain. The arrows indicate 3 typical instances of axonal leakage, showing a dark center with a diffuse halo. D: Intact labeled cortical fibers and a few slightly swollen axons (arrowhead) in a non-demented case (61 years old, Netherlands Brain Bank number 96-081). The arrow indicates the normal axon of a labeled neuron. Scale bars: 50 μm.

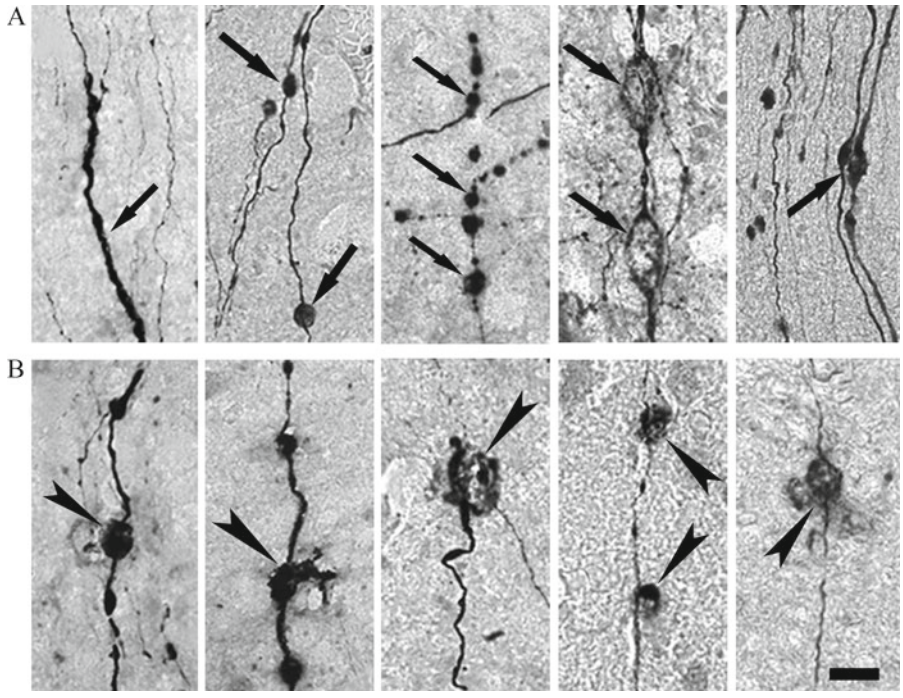

Fig. 2 Profiles of swollen axons and varicosities, and axonal leakage. A: Different examples of profiles of swollen axons and varicosities on swollen axons without obvious axonal leakage (arrows) in the cortex of Alzheimer's disease (AD) brains. B: Different examples of typical instances of axonal leakage (arrowheads) in the cortex of AD brains. Scale bar: 25 μm.

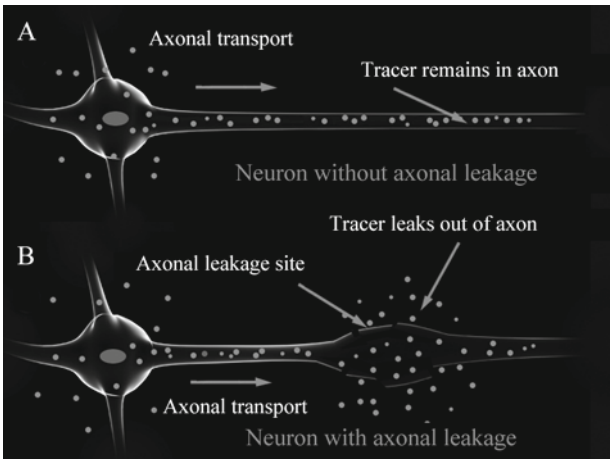

Fig. 3 A diagram explaining the identification of axonal leakage using the tracing technique. The tracer is taken up by a neuron, transported along its axon and eventually reaches the terminals. In a normal neuron, the tracer remains in the axon, and the staining pattern resembles A. If the axon is damaged, the tracer leaks from the axon, and the staining pattern resembles B.

from human postmortem brain, such as postmortem delay, age, sex, and agonal state (e.g. cause of death). In addition, based on the previous finding that variations in the size of tracer injection influence the pattern and the number of labeled fibers[17] thus affecting the number of instances of axonal leakage, here cases with similar tracer injection size and labeling pattern were selected (Fig. 5B). The mean injection sizes were (0.943 ± 0.068) mm (mean ± SD, n = 4) in FC and (0.955 ± 0.054) mm (n = 4) in TC from non-demented subjects, and no significant difference was found (P = 0.889). The mean injection sizes were (0.981 ± 0.080) mm (n = 8) in FC and (0.976 ± 0.059) mm (n = 8) in TC from AD subjects, also with no significant difference (P = 0.785). However, the number of instances of axonal leakage in TC was significantly larger than that in FC in AD subjects (P = 0.008) (Fig. 5A, Table 2). This might be related to the neuropathological changes such as SPs and NTFs, as SPs and NFTs were denser in TC than in FC (Table 2). In contrast, the mean number of instances of axonal leakage was not significantly different between FC and TC in non-demented control subjects (P = 0.094) (Fig. 5A).

3.3 The relationship between axonal leakage and classical neuropathological changes The relationship between axonal leakage and the classic neuropathological changes, SPs and NFTs, was investigated. To address whether axonal leakage is an early event in the origin and development of SPs and NFTs, or an independent neuropathological change, here double immunohistochemical

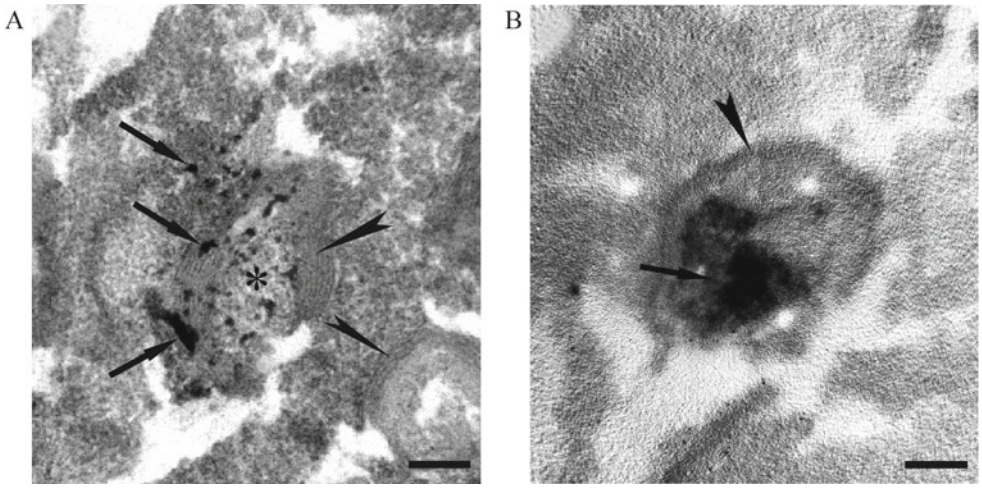

Fig. 4 Ultrastructural profile of axonal leakage and intact axon. A: Ultrastructural profile of axonal leakage, showing labeled tracer in the intra-axonal space (asterisk) and extra-axonal space. The top arrow indicates the presence of tracer in the extra-axonal space, and the other arrows indicate the presence of the tracer within the myelin sheath. The 2 arrowheads indicate the myelin sheaths of labeled (upper) and non-labeled (lower) axons, respectively. B: Ultrastructural profile of an intact axon, showing labeled tracer in the intra-axonal space (arrow). The arrowhead indicates the myelin sheath. Scale bars: 0.2 μm.

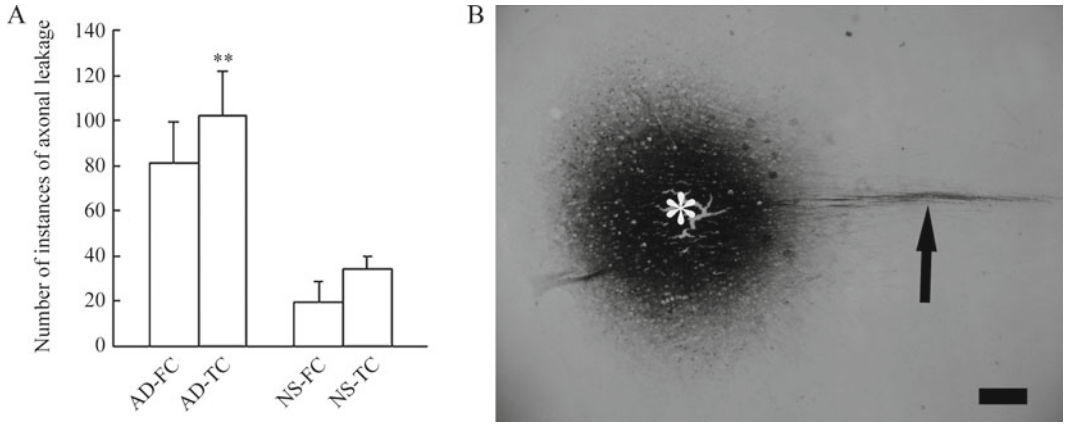

Fig. 5 Degrees of axonal leakage in the frontal cortex (FC) and temporal cortex (TC) in Alzheimer's disease (AD) and control brains. A: Mean numbers of instances of axonal leakage in FC and TC from 8 AD and 4 non-demented subjects (NS). The mean number of instances of axonal leakage in TC was significantly larger than that in FC in AD subjects ($P = 0.008$), while there was no difference in the NS group ($P = 0.094$). $^{**}P < 0.01$. B: A tracer (biotinylated dextran amine) injection spot in a TC slice from an AD patient (Netherlands Brain Bank number 96-131). The labeled fibers run into the white matter (arrow). The asterisk indicates the injection center. Scale bar: 200 μm.

Table 2. Numbers of instances of axonal leakage in FC and TC of AD and non-demented subjects (NS) after one-site tracer injection, and intensity of SPs and NFTs in the same brain regions

NBBn	Dia	Age (y)	Sex	Bw (g)	Pmd (h:m)	CSF (pH)	ApoE	Braak	FC			TC		
									AL	SPs	NFTs	AL	SPs	NFTs
96-054	AD	87	F	1010	6:55	6.96	43	5	35.6±9.9	1	1	86.8±6.5	2	2
96-066	AD	91	F	949	4:35	6.55	43	6	122.9±10.0	1	3	171.5±16.3	3	3
96-070	AD	83	F	1007	4:00	6.73	43	5	77.9±2.9	1	1	82.4±7.8	2	2
96-110	AD	80	F	1195	5:45	6.51	43	6	7.9±1.7	1	2	29.4±2.7	3	3
96-115	AD	92	F	964	2:50	6.64	33	5	119.3±8.7	2	2	136.6±11.2	3	3
96-123	AD	88	F	1004	3:20	6.52	ND	4	24.9±1.9	1	1	29.5±9.7	2	3
96-130	AD	87	F	955	4:00	6.91	43	4	153.9±14.8	1	1	166.6±18.7	3	3
96-131	AD	87	F	1368	4:05	6.71	33	3	59.8±7.1	2	0	102.5±8.4	3	1
96-067	NS	70	F	1157	10:30	ND	33	1	6.9±0.9	0	0	17.4±1.4	0	0
96-078	NS	87	F	1315	8:00	6.91	33	2	16.8±3.4	1	0	41.3±1.6	1	1
96-084	NS	78	F	1330	7:30	6.60	43	2	45.4±1.7	0	0	44.6±6.4	0	1
96-085	NS	84	M	1367	9:00	6.20	33	1	10.5±1.7	0	1	31.8±5.8	0	0

SPs and NFTs were scored as none (0), sparse/slight (1), moderate (2) or frequent/severe (3). AL: axonal leakage (mean ± SE); SPs: senile plaques; NFTs: neurofibrillary tangles; FC: frontal cortex; TC: temporal cortex; AD: Alzheimer's disease; NS: non-demented subjects; NBBn: Netherlands Brain Bank number; M: male; F: female; Dia: clinical diagnosis; Bw: brain weight; Pmd: postmortem delay; h:m: hours:minutes; CSF: cerebral spinal fluid; ApoE: apolipoprotein gene type; Braak: Braak stage; ND: not detected.

and immunofluorescence staining for tracer and Aβ (Aβ42), P-tau, tau-5 or AT8 were performed. As shown in Fig. 6, Aβ42 and hyperphosphorylated tau staining were located within and/or close to the swollen axons, varicosities or

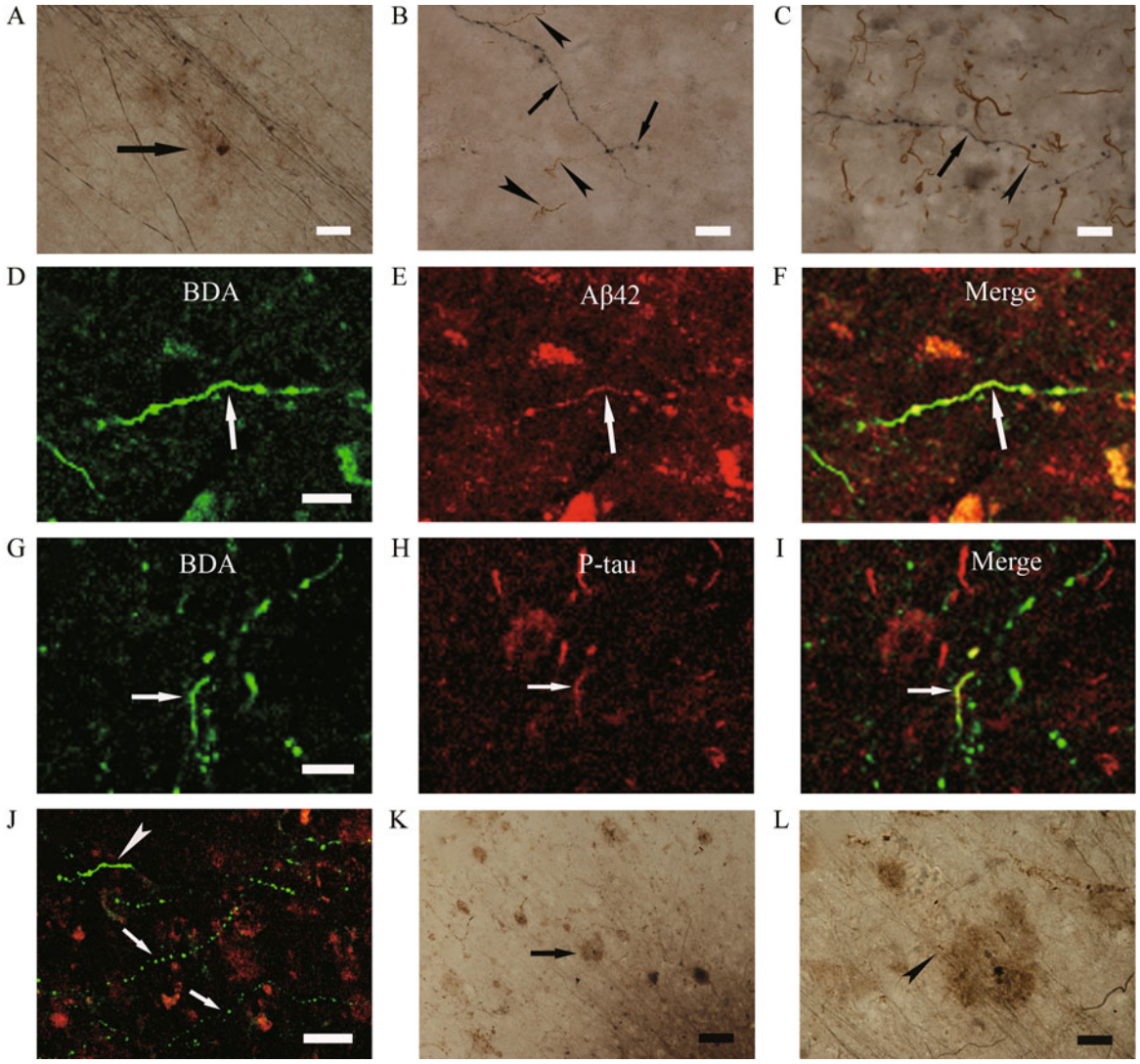

Fig. 6 Morphological relationship between axonal leakage and SPs or NFTs in the prefrontal and the temporal cortices in AD brains. A: Swollen fibers with tracer labeling (dark blue) and diffuse Aβ42 staining (brown, arrow). B: Two fibers labeled with tracer (dark blue, arrows) and fiber branches labeled with Aβ42 staining (brown, arrowheads). C: A swollen fiber labeled with tracer (dark blue, arrow) presented P-tau staining on one side (brown, arrowhead). D–F: Double immunofluorescence staining presented Aβ42 (red) in a swollen fiber labeled with tracer (BDA, green). G–I: Part of a swollen fiber labeled with tracer (green, arrow) presenting P-tau staining (red, arrow). J: Double immunofluorescence staining presented tracer-labeled slightly swollen (arrowhead, green) and normal fibers (arrow, green) associated with Aβ42-positive plaques (red). K, L: The relationship between tracer-labeled fibers (dark blue) and Aβ42-positive plaques (brown). Normal fibers (arrowhead in H) passed through a plaque (arrow in K). L is the magnification of an area in K. Scale bars: 100 μm for K; 25 μm for A and J; and 10 μm for B–I and L. BDA: biotinylated dextran amine.

axonal terminals associated with axonal leakage. Besides, a segment of axon exhibiting hyperphosphorylated tau staining merged with a tracer-labeled "normal fiber" (Fig. 6C, G–I). In addition, double immunohistochemical and immunofluorescence staining against Aβ and hyperphosphorylated tau (P-tau and AT8) showed that the formation and development of classic Aβ plaques were often associated with axonal changes. Even very small plaques contained extensive large swollen axons and varicosities with tau staining (Fig. 7). Interestingly, normal fibers or terminals labeled by tracer were detectable in the plaques in the brains of AD patients (Fig. 6J–L).

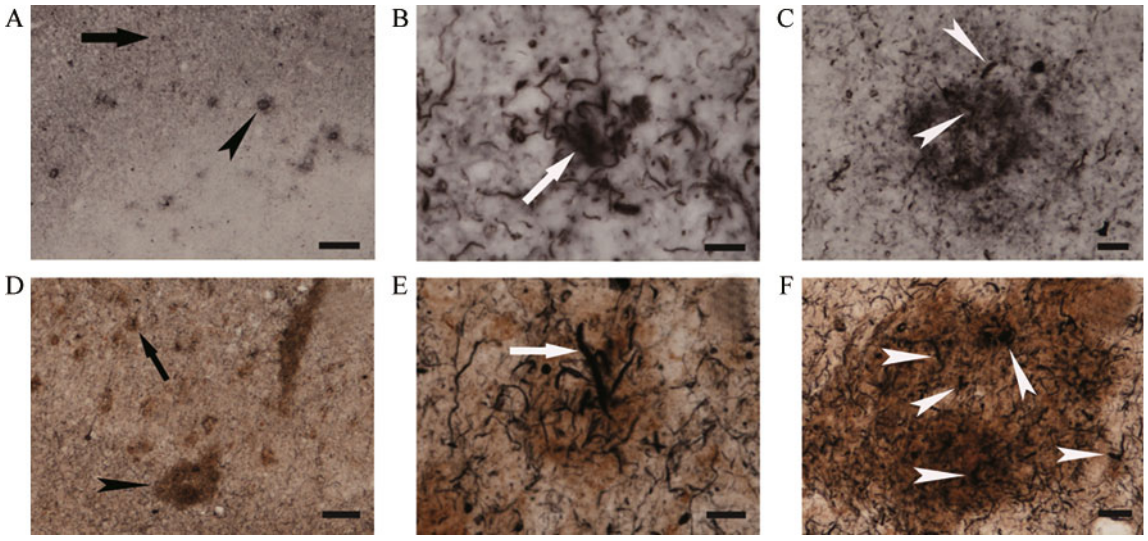

Fig. 7 Axonal changes related to the formation and development of senile plaques (SPs) and neurofibrillary tangles (NFTs) in Alzheimer's disease (AD) brains. A: P-tau immunostaining presented "plaque-like" patterns in the temporal cortex of an AD brain. B: A few swollen axons and varicosities (arrow in B) were present in a very small "plaque-like" P-tau staining area (arrow in A) at high magnification. C: A medium-sized "plaque-like" P-tau staining area (arrowhead in A) contained more swollen axons and varicosities at high magnification (arrowheads). D: Double staining for Aβ42 (brown) and AT8 (dark blue) showed the plaques of different sizes. E: A few large swollen axons (arrow) occured in a very small plaque (Aβ42 staining, arrow in D) at high magnification. F: Many swollen axons and varicosities (arrowheads) at a larger plaque (arrowhead in D) at high magnification. Scale bars: 200 μm for A; 100 μm for D; 20 μm for C and F; 10 μm for B and E.

4 Discussion

The *in vitro* postmortem tracing technique has been used to study hypothalamic neural circuits (neural connections) and axonal transport in human brains[17, 18, 31]. In the present study, the use of this technique in human brain materials was extended to analyze changes in axon morphology, which are related to the neuropathological mechanisms underlying AD. With proper *in vitro* treatment, human brain cells, even those with a postmortem delay of up to 10 h, can survive to an extent that they still have the potential of recovering axonal transport[31] and present axon morphology similar to that observed by *in vivo* tracing techniques. In addition, the tissue fixation used in the present study did not result in obvious changes in axon morphology. Therefore, the observed axonal changes were not an artifact due to the relatively long incubation time (up to 6–8 h) or tissue fixation used during *in vitro* postmortem tracing. It should be emphasized that the cause of death, mostly pneumonia, cachexia and dehydration in AD, may not be the main cause of axonal leakage, since axon morphology is quite normal in some brain areas such as visual cortex in most AD cases, although evident axonal changes, including axonal leakage, occur in TC and FC.

In the present study, we investigated axonal leakage in the brains of AD patients, and analyzed its relationship with the classic neuropathologcal changes, SPs and NFTs. Stokin *et al.* have revealed that axonal swellings are precursors in AD, and that they precede amyloid deposits and other disease-related neuropathies[19]. Our findings are consistent with that report. Together with previous findings, our data suggest that axonal leakage may be an important initial neuropathological change leading to the origin and development of the classic neuropathies, SPs and NFTs, as well as cognitive defects in AD. Although the detailed mechanism of how axonal leakage results in the formation and development of SPs and NFTs needs to be investigated, the possible explanations are as follows.

Direct leakage of intra-axonal components, including structural and functional proteins, to extra-axonal space may be partly involved in the formation of plaques. For example, the leakage of overproduced intra-axonal Aβ or

extra-axonal proteolysis of the leaked amyloid precursor protein may result in Aβ plaques[33], which may explain the Aβ plaques observed in brain areas with unimpaired neural functions[2,11]. Axonal leakage may be present at axon terminals of affected neurons located far from their termination areas, however, these areas may still exhibit unimpaired function if their neurons are not affected despite the presence of plaques. For example, if affected entorhinal cortex neurons undergo axonal leakage in their projection areas in the TC and FC, plaques may form in the projection areas. Such an explanation is supported by our finding that intact neural fibers were present in or around the plaques (Fig. 6J–L). We also observed degenerating neuronal fibers around the plaques, which is similar to the previous findings (Fig. 6K, L). This is probably because these fibers arise from affected neurons, although we cannot exclude the possibility that this may be due to the neurotoxic effects of Aβ[6,24,34]. In another study, Meyer-Luehmann *et al*. demonstrated in a mouse model of AD that plaques can grow overnight, with mature plaques originating from smaller amyloid deposits (microplaques) associated with alterations in neighboring neurites[35]. The origin of the microplaques is unclear, but our recent findings suggest that they might be related to axonal leakage.

Axonal leakage may result in an abnormal change in intra-axonal Ca^{2+} concentration due to uncontrolled direct diffusion from extra-axonal to intra-axonal space. This may induce tau hyperphosphorylation through activation of a Ca^{2+}-dependent enzyme, a key step in the formation of NFTs[36,37]. This explanation is supported by our finding that hyperphosphorylated tau staining occured in certain segments of a relatively normal axon. In this situation, axonal leakage may be at an early and reversible stage. This also suggests that NFTs originate earlier than SPs[5,11,38,39].

Our findings also provide a better understanding of the relationship between the AD-related risk factors and the neuropathies of this disease. Axonal leakage is likely due to alterations in the axonal membrane and myelin sheath. Therefore, we propose that AD-like neuropathological changes and cognitive deficits might be expected if any of the risk factors such as mitochondrial dysfunction, abnormal metabolism and oxidative stress affects the membrane stability and consequently induces severe axonal leakage[18,40,41]. Although the cellular and molecular mechanisms underlying the origin and development of axonal leakage are not yet understood, disruption in the function of oligodendrocytes (including their precursor cells) as well as their integration with neurons and astrocytes may play an important role[42]. Therefore, reducing axonal leakage by stabilizing, strengthening and enriching the neuronal membrane and myelin sheath may provide a new strategy for prevention of AD, as well as a potential therapy for this disease.

Acknowledgements: This work was supported by an "Excellent Project" of the China Ministry of Human Resources for Return Overseas Chinese Scholarship, partly by the Research Foundation for "Key Laboratory of Neuroscience and Neuroengineering" of South-Central University for Nationalities (No. XJS09001) and the National Natural Science Foundation of China (No. 31070961).

References:

[1] Masliah E, Mallory M, Deerinck T, DeTeresa R, Lamont S, Miller A, *et al*. Re-evaluation of the structural organization of neuritic plaques in Alzheimer's disease. J Neuropathol Exp Neurol 1993, 52: 619–632.

[2] Goedert M. Tau protein and the neurofibrillary pathology of Alzheimer's disease. Trends Neurosci 1993, 16: 460–465.

[3] Hardy J, Allsop D. Amyloid deposition as the central event in the aetiology of Alzheimer's disease. Trends Pharmacol Sci 1991, 12: 383–388.

[4] Armstrong RA, Myers D, Smith CUM. The spatial patterns of plaques and tangles in Alzheimer's disease do not support the 'Cascade hypothesis'. Dementia 1993, 4: 16–20.

[5] Terry RD. The pathogenesis of Alzheimer disease: an alternative to the amyloid hypothesis. J Neuropathol Exp Neurol 1996, 55: 1023–1025.

[6] Neve RL, Robakis NK. Alzheimer's disease: a re-examination of the amyloid hypothesis. Trends Neurosci 1998, 21: 15–19.

[7] Hardy J, Selkoe DJ. The amyloid hypothesis of Alzheimer's disease: progress and problems on the road to therapeutics. Science 2002, 297: 353–356.

[8] Mudher A, Lovestone S. Alzheimer's disease–do tauists and bap-

tists finally shake hands? Trends Neurosci 2002, 25: 22–26.

[9] Duyckaerts C. Looking for the link between plaques and tangles. Neurobiol Aging 2004, 25: 735–739.

[10] Mattson MP. Pathways towards and away from Alzheimer's disease. Nature 2004, 430: 631–639.

[11] Schönheit B, Zarski R, Ohm TG. Spatial and temporal relationships between plaques and tangles in Alzheimer-pathology. Neurobiol Aging 2004, 25: 697–711.

[12] Tanzi RE, Bertram L. Twenty years of the Alzheimer's disease amyloid hypothesis: a genetic perspective. Cell 2005, 120: 545–555.

[13] Trojanowski JQ, Lee VMY. The Alzheimer's brain binding out what's broken tells us how to fix it. Am J Pathol 2005, 167: 1183–1188.

[14] Armstrong RA. The pathogenesis of Alzheimer's disease: a reevaluation of the "amyloid cascade hypothesis". Int J Alzheimers Dis 2011, 2011: 630865.

[15] Schwartz JH. Axonal transport: components, mechanisms, and specificity. Annu Rev Neurosci 1979, 2: 467–504.

[16] Hirokawa N. Kinesin and dynein superfamily proteins and the mechanism of organelle transport. Science 1998, 279: 519–526.

[17] Dai J, Buijs RM, Kamphorst W, Swaab DF. Impaired axonal transport of cortical neurons in Alzheimer's disease is associated with neuropathological changes. Brain Res 2002, 948: 138–144.

[18] Dai J, Buijs RM, Swaab DF. Glucocorticoid hormone (cortisol) affects axonal transport in human cortex neurons but shows resistance in Alzheimer's disease. Br J Pharmacol 2004, 143: 606–610.

[19] Stokin GB, Lillo C, Falzone TL, Brusch RG, Rockenstein E, Mount SL, *et al.* Axonopathy and transport deficits early in the pathogenesis of Alzheimer's disease. Science 2005, 307: 1282–1288.

[20] Stokin GB, Goldstein LS. Axonal transport and Alzheimer's disease. Annu Rev Biochem 2006, 75: 607–627.

[21] Smith KD, Kallhoff V, Zheng H, Pautler RG. *In vivo* axonal transport rates decrease in a mouse model of Alzheimer's disease. Neuroimage 2007, 35: 1401–1408.

[22] Lazarov O, Morfini GA, Pigino G, Gadadhar A, Chen X, Robinson J, *et al.* Impairments in fast axonal transport and motor neuron deficits in transgenic mice expressing familial Alzheimer's disease-linked mutant presenilin 1. J Neurosci 2007, 27: 7011–7020.

[23] Minoshima S, Cross D. *In vivo* imaging of axonal transport using MRI: aging and Alzheimer's disease. Eur J Nucl Med Mol Imaging 2008, 35(Suppl 1): S89–92.

[24] Adalbert R, Nogradi A, Babetto E, Janeckova L, Walker SA, Kerschensteiner M, *et al.* Severely dystrophic axons at amyloid plaques remain continuous and connected to viable cell bodies. Brain 2008, 132: 402–416.

[25] Vickers JC, King AE, Woodhouse A, Kirkcaldie MT, Staal JA, McCormack GH, *et al*. Axonopathy and cytoskeletal disruption in degenerative diseases of the central nervous system. Brain Res Bull 2009, 80: 217–223.

[26] Muresan V, Muresan Z. Is abnormal axonal transport a cause, a contributing factor or a consequence of the neuronal pathology in Alzheimer's disease? Future Neurol 2009, 4: 761–773.

[27] Massaad CA, Amin SK, Hu L, Mei Y, Klann E, Pautler RG. Mitochondrial superoxide contributes to blood flow and axonal transport deficits in the Tg2576 mouse model of Alzheimer's disease. PLoS One 2010, 5: e10561.

[28] Xiao A, Dai J. Axonal leakage is a key neuropathological change in Alzheimer's disease. Acta Med Univ Sci Technol Huazhong 2006, 35: 277–278 (in Chinese).

[29] McKhann G, Drachman D, Folstein M, Katzman R, Price D, Stadlan EM. Clinical diagnosis of Alzheimer's disease: report of the NINCDS-ADRDA Work Group under the auspices of Department of Health and Human Services Task Force on Alzheimer's disease. Neurology 1984, 34: 939–944.

[30] Braak H, Braak E. Demonstration of amyloid deposits and neurofibrillary changes in whole brain sections. Brain Pathol 1991, 1: 213–216.

[31] Dai J, Swaab DF, Van der Vliet J, Buijs RM. Postmortem tracing reveals the organization of hypothalamic projections of the suprachiasmatic nucleus in the human brain. J Comp Neurol 1998, 400: 87–102.

[32] Erisir A, Aoki C. A method of combining biocytin tract-tracing with avidin-biotin-peroxidase complex immunocytochemistry for pre-embedding electron microscopic labeling in neonatal tissue. J Neurosci Methods 1998, 81: 189–197.

[33] Nunan J, Small DH. Regulation of APP cleavage by α-, β-, and γ -secretases. FEBS Lett 2000, 483: 6–10.

[34] Shah SB, Nolan R, Davis E, Stokin GB, Niesman I, Canto I, *et al.* Examination of potential mechanisms of amyloid-induced defects in neuronal transport. Neurobiol Dis 2009, 36: 11–25.

[35] Meyer-Luehmann M, Spires-Jones TL, Prada C, Garcia-Alloza M, de Calignon A, Rozkalne A, *et al.* Rapid appearance and local toxicity of amyloid-beta plaques in a mouse model of Alzheimer's disease. Nature 2008, 415: 720–725.

[36] Steiner B, Mandelkow EM, Biernat J, Gustke N, Meyer HE, Schmidt B, *et al.* Phosphorylation of microtubule-associated protein tau: identification of the site for Ca^{2+}-calmodulin dependent kinase and relationship with tau phosphorylation in Alzheimer tangles. EMBO J 1990, 9: 3539–3544.

[37] Fleming LM, Johnson GV. Modulation of the phosphorylation state of tau *in situ*: the roles of calcium and cyclic AMP. Biochem J 1995, 309: 41–47.

[38] Cras P, Kawai M, Lowery D, Gonzalez-DeWhitt P, Greenberg B, Perry G. Senile plaque neurites in Alzheimer disease accumulate amyloid precursor protein. Proc Natl Acad Sci U S A 1991, 88: 7552–7556.

[39] Rifenburg RP, Perry G. Dystrophic neurites define diffuse as well as core-containing senile plaques in Alzheimer's disease. Neurodegeneration 1995, 4: 235–237.
[40] Lin MT, Beal MF. Mitochondrial dysfunction and oxidative stress in neurodegenerative diseases. Nature 2006, 443: 787–795.
[41] Muhammad S, Bierhaus A, Schwaninger M. Reactive oxygen species in diabetes-induced vascular damage, stroke, and Alzheimer's disease. J Alzheimers Dis 2009, 16: 775–785.
[42] Salmina AB. Neuron-glia interactions as therapeutic targets in neurodegeneration. J Alzheimers Dis 2009, 16: 485–502.

阿尔茨海默病老年斑及磷酸化 tau 蛋白的形成和发展与轴突病变相关

肖爱武[1]，何敬[1]，王茜[1,2]，罗艺[1]，孙燕[1]，周艳平[1]，官阳[3]，Paul J. Lucassen[2]，戴甲培[1]

[1] 中南民族大学武汉神经科学和神经工程研究所，武汉 430074
[2] 阿姆斯特丹大学生命科学研究所神经科学研究中心，阿姆斯特丹 1098XH，荷兰
[3] 华中科技大学同济医学院病理学系超微病理研究室，武汉 430030

摘要：目的 神经毒性β-淀粉样蛋白沉积和tau蛋白过度磷酸化是阿尔茨海默病(Alzheimer’s disease, AD)神经病理机制的两个关键阶段，然而关于它们在启动AD病程的重要性上仍存在争议。最近研究显示，轴突病变发生于AD的早期，然而轴突病变与老年斑(senile plaques, SPs)和神经纤维缠结(neurofibrillary tangles, NFTs)的发生发展之间的确切关系仍不清楚，本研究旨在揭示它们之间的联系。**方法** 运用神经示踪技术结合免疫组织化学、免疫组织化学和免疫荧光双标技术，研究AD患者大脑中的轴突病变以及SPs和NFTs的形成情况。**结果** AD患者的脑组织中呈现出一种新形式的轴突病变——“轴突漏”，并伴随有大量肿胀的轴突和膨体。此外，轴突漏与β-淀粉样蛋白沉积和tau蛋白过度磷酸化的形成及发展有关。**结论** 轴突病变尤其是“轴突漏”可能是起始AD神经病理进程的一个关键事件。

关键词：阿尔茨海默病；轴突病变；老年斑；神经纤维缠结；离体示踪